Letter

Superconductivity-enhanced spin pumping: Role of Andreev resonances

Mostafa Tanhayi Ahari and Yaroslav Tserkovnyak
Department of Physics and Astronomy, University of California, Los Angeles, California 90095, USA

(Received 11 September 2020; accepted 22 February 2021; published 15 March 2021)

We describe a simple hybrid superconductor–ferromagnetic-insulator structure manifesting spin-resolved Andreev bound states in which dynamic magnetization is employed to probe spin related physics. We show that, at low bias and below T_c, the transfer of spin angular momentum pumped by an externally driven ferromagnetic insulator is greatly affected by the formation of spin-resolved Andreev bound states. Our results indicate that these bound states capture the essential physics of condensate-facilitated spin flow. For finite thicknesses of the superconducting layer, comparable to the coherence length, resonant Andreev bound states render highly transmitting subgap spin transport channels. We point out that the resonant enhancement of the subgap transport channels establishes a prototype Fabry-Pérot resonator for spin pumping.

DOI: 10.1103/PhysRevB.103.L100406

I. INTRODUCTION

Spatial variations in the superconducting order in a finite region lead to the formation of spin-degenerate Andreev bound states (ABSs) with discrete excitation energies below the superconducting gap [1]. An externally applied magnetic field or proximity to a ferromagnetic order, on the other hand, can induce spin splitting in the ABSs that results in spin-resolved ABSs [2]. In this paper, we consider a normal metal (N) sandwiched between a superconductor (S) and a ferromagnetic insulator (FI) that serves as a simple platform with spin-resolved ABSs, which are localized in the N layer. The nonequilibrium pure spin current engendered from the externally driven FI—spin pumping—is utilized to probe spin transport in an S-N-FI hybrid structure. The spin pumping generated from a time-dependent magnetization, on the other hand, is a flow of spin angular momentum into adjacent materials that dissipates energy of the ferromagnet [3]. We suggest that the magnetic damping increase in superconducting hybrid multilayers Nb-$Ni_{80}Fe_{20}$ and NbN-GdN reported, respectively, in Refs. [4] and [5] may be attributed to the resonant enhancement of the spin pumping discussed here.

In the context of superconducting spintronics, combining an *s*-wave superconducting order, favoring electrons to form a singlet state, with a ferromagnetic order, favoring spin alignment, leads to a powerful enhancement or reduction of angular momentum transfer [6,7]. The angular momentum transfer, as a central effect in spintronics, is greatly modified on account of two major underlying causes: the itinerant spin-polarized quasiparticles (QPs) with long spin-coherence lengths [8,9] and the creation of spin-triplet Cooper pairs [10–12] induced at highly spin-active regions or complex magnetic multilayers [13]. Here, the spin pumping in an S-N-FI hybrid structure, however, is an interplay between spin-polarized QPs and spin-triplet Cooper pairs, which are dynamically generated by the excited FI [14,15]. The subgap ABSs accommodate the spin-polarized QPs and spin-triplet Cooper pairs that for a sufficiently thin S layer can tunnel across and contribute to the spin current. To collect the spin current we have placed a spin reservoir N_r, comprising an N_r-S-N-FI structure (see Fig. 1). While spin pumping has been considered as a new probe of spin dynamics in a superconducting thin film [16] and tunable pure spin supercurrents [17], here we propose to study spin-resolved Andreev resonances by means of spin pumping.

II. SPIN-RESOLVED ABS

We will determine the subgap spin-resolved ABSs by studying the resonant conditions for the spin transport in an N_r-S-N-FI hybrid structure. In order to establish the pumped spin current in the presence of superconducting and dynamic ferromagnetic orders, we solve a time-dependent scattering problem [15,18], which accounts for the relevant processes such as Andreev reflection (AR), ABS, and a dynamic triplet-paring generation. For subgap energies, the full scattering matrix develops peak structures marking resonant bound states [19] (ABSs), which result in highly transmitting subgap transport channels for the spin flow. While we identify the Andreev resonances in the ballistic regime, we do not expect their perturbation by a weak disorder to significantly modify the spectroscopic aspects of spin pumping (which should be governed by the underlying dynamic mixing between the superconducting singlet and triplet components). To capture the essential effect of interfacial scattering on the spin-pumping enhancement, we will consider an interface disorder at $x = d_S$.

We proceed with establishing notations and key features of the scattering. The incident QPs from the reservoir onto the N_r-S interface can either transmit across the S or reflect as holes back into the reservoir, a process known as AR. The AR amplitude for an incident QP with energy ε is given by

$$r_A^\infty = \begin{cases} e^{-i\arccos(\varepsilon/\Delta)}, & |\varepsilon| < \Delta \\ \frac{\varepsilon - \varepsilon\sqrt{1-\Delta^2/\varepsilon^2}}{\Delta}, & |\varepsilon| > \Delta \end{cases}, \tag{1}$$

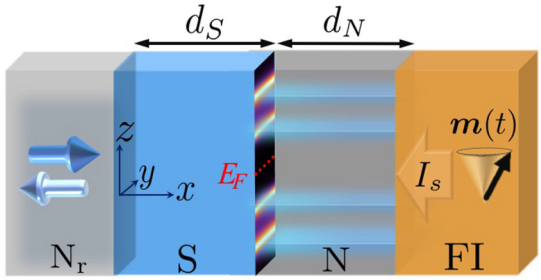

FIG. 1. Schematic sketch for an N_r-S-N-FI hybrid structure. The FI region with precessing magnetization $\boldsymbol{m}(t)$ injects spin angular momentum, I_s, that is carried by the QPs into the reservoir N_r (spin pumping). For finite thicknesses of the S and N layers ($d_S, d_N \sim$ coherence length) the resonant ABSs provide highly transmitting transport channels for spin pumping. Here, for example, we show four resonant channels with two positive-energy ABSs. The energies are measured with respect to the Fermi energy E_F depicted in the middle.

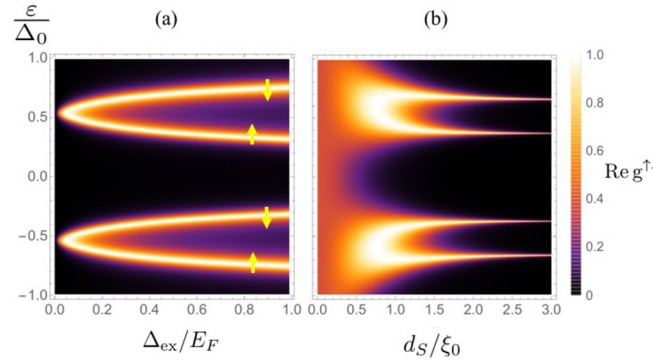

FIG. 2. Profile of $\mathrm{Re}\, g^{\uparrow\downarrow}$ for $d_N/\xi_0 = 1$. (a) Assuming fixed S layer thickness ($d_S/\xi_0 = 1.5$), the spectral overlap of the spin-split Andreev levels can be modified by Δ_{ex}. (b) At the finite thicknesses of the S, $d_S \gtrsim \xi_0$, the Andreev resonances establish highly transmitting transport channels. Here, we have set $\Delta_{ex}/E_F = 0.4$.

where Δ is the superconducting pair potential [20]. The AR amplitude given in Eq. (1), by focusing on the interface, assumes a bulk S (a thick S layer) [15]. A nonzero probability of QP transmission for the thin S as well as an interfacial disorder can reduce the AR probability, which we address below. The transmitted QPs with spin $\sigma \in \{\uparrow, \downarrow\}$ propagate through the normal metal junction and acquire a spin-dependent phase $e^{i\vartheta_\sigma}$ upon reflection from the FI interface, where the FI region is considered an exchange-splitting insulator for the QPs [21]. This renders the full scattering matrix to be merely a reflection matrix, which is block diagonal in the spin space due to the conservation of the QP spin during each individual scattering event. Consequently, multiple ARs at the N-S along with spin-dependent reflections at the N-FI interfaces constitute the full scattering matrix.

The spin-active interface N-FI, upon reflection, rotates a noncollinear QP spin around the FI magnetization axis, which in turn for a driven magnetization leads to generation of a nonequilibrium spin current detected in N_r [22]. The conductance determining the transport of this spin current, known as the mixing conductance $g^{\uparrow\downarrow}$, is given by

$$\mathrm{g}^{\uparrow\downarrow} = \sum_{n,m} \left(\delta_{m,n} - r^{\uparrow}_{ee,mn}\, r^{\downarrow *}_{ee,mn} + r^{\uparrow}_{he,mn}\, r^{\downarrow *}_{he,mn}\right), \qquad (2)$$

where r^{σ}_{ee} and r^{σ}_{he} represent the total spin-σ electron-to-electron and electron-to-hole reflection matrices in the S|N|FI hybrid structure, respectively [14,18]. The indices n and m refer to transport channels the number of which can be determined by transverse thickness of the normal metal layer [20]. The reflection matrices in Eq. (2) are written in the basis where the spin quantization axis is parallel to the magnetization in the FI (the exact expressions for the reflection amplitudes in the ballistic regime can be found in the Supplemental Material [15]). In the following, we provide the results for the single-channel scattering and postpone discussing the case of multichannel scattering to the Supplemental Material [15].

Generically, the mixing conductance given in Eq. (2) is a complex number the real part of which governs the average spin pumping and the associated Gilbert damping [18]. After a straightforward calculation in the ballistic regime, three distinct regimes are recognized for subgap energies:

$$\mathrm{Re}\, g^{\uparrow\downarrow} \approx \begin{cases} 1 - \cos\vartheta & d_S \ll \xi_0 \\ \gamma^2/(\gamma^2 + \beta^2) & d_S \sim \xi_0 \\ 0 & d_S \gg \xi_0 \end{cases}, \qquad (3)$$

where $\gamma = \exp[-2\sqrt{1 - \varepsilon^2/\Delta_0^2}\, d_S/\xi_0]$, $\beta = [\cos(4d_N\varepsilon/\xi_0\Delta_0 + 2\theta_A) - \cos\vartheta]/4\sin\vartheta\, \sin^2\theta_A$, and $\theta_A \equiv -\arccos(\varepsilon/\Delta_0)$. The mixing angle defined as $\vartheta \equiv \vartheta_\uparrow - \vartheta_\downarrow$ is controlled by the FI exchange interaction Δ_{ex} [15]. Here, Δ_0 and ξ_0 are the superconducting gap and coherence length at zero temperature, respectively. Evidently, $\mathrm{Re}\, g^{\uparrow\downarrow}$ displays a resonant behavior associated with the intermediate S thickness. The resonant energy levels correspond to the ABS energies ε_A determined by ($\beta = 0$):

$$\varepsilon_A = \Delta_0\, \mathrm{sign}\left[\sin\left(\frac{2d_N\varepsilon_A}{\xi_0\Delta_0} \pm \frac{\vartheta}{2}\right)\right] \cos\left(\frac{2d_N\varepsilon_A}{\xi_0\Delta_0} \pm \frac{\vartheta}{2}\right). \qquad (4)$$

When the exchange interaction is absent, that is, $\vartheta = 0$, Eq. (4) yields a pair of solutions $(-\varepsilon_A, \varepsilon_A)$, which is a consequence of the particle-hole symmetry imposed on the scattering formalism [15]. A nonzero mixing angle ϑ, on the other hand, by lifting the spin degeneracy of each level results in the spin-resolved ABSs with the following energies $(-\varepsilon_A^{\pm}, \varepsilon_A^{\pm})$. As an outcome, the spectral overlap of the spin-split bound states can be controlled by the exchange interaction of the FI [e.g., see Fig. 2(a)]. We emphasize that, following Eq. (3), only at $d_S \sim \xi_0$ the resonant ABSs establish highly transmitting transport channels for the spin flow, which is greatly enhanced compared to either a bulk or no S layer [see Fig. 2(b)]. This is one of the main results of this paper.

In the limit where $d_N \to 0$, Eq. (4) can be reduced to the well-known result [23] for ABSs with magnetically active interfaces, $\varepsilon_A/\Delta_0 = \pm\cos\vartheta/2$. We highlight the fact that Eq. (4) is a condition for a constructive quantum interference in a Rowell-McMillan process for the QPs [12], that is, four times crossing N with two Andreev conversions as well as two reflections from FI, once as electron and once as hole. It is clear that a constructive interference for QPs inside the

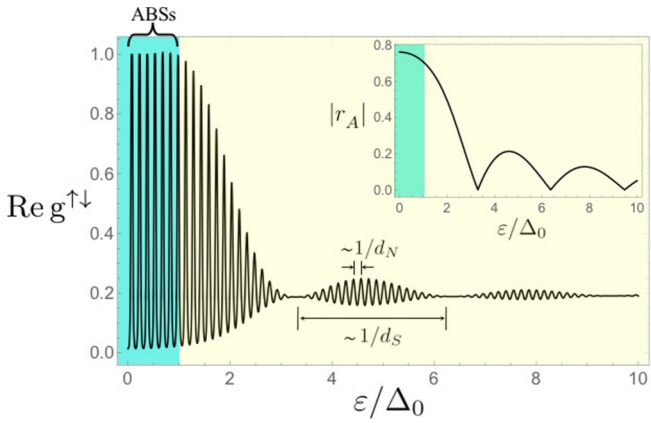

FIG. 3. Geometric resonances of $\mathrm{Re}\, g^{\uparrow\downarrow}$. The Fabry-Pérot oscillations happen when the corresponding AR probability $|r_A|$ is nonzero (the inset plot shows the probability of AR vs energy). For a fixed Δ_{ex}, the Fabry-Pérot oscillations are determined by d_N that for $\varepsilon > \Delta_0$ get modulated with a frequency determined by d_S (i.e., energies for which $|r_A| = 0$). Here, we have adopted the following parameters: $d_S/\xi_0 = 1$, $d_N/\xi_0 = 10$, and $\Delta_{\mathrm{ex}}/E_F = 0.2$.

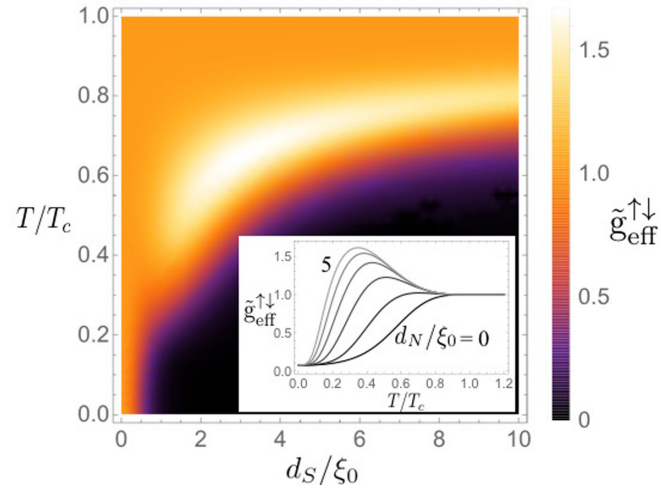

FIG. 4. The normalized effective conductance, $\tilde{g}^{\uparrow\downarrow}_{\mathrm{eff}}$, for subgap temperatures and intermediate thickness $d_S \sim \xi_0$ showing a significant enhancement relative to the normal case near T_c. As the S gap shrinks, with the increase of temperature, the enhancement peak location creeps up to higher d_S, which ultimately diminishes for higher temperatures near T_c. Here, we have set $d_N/\xi_0 = 2.5$. The inset shows that the enhancement feature happens for all $0 \leqslant d_N/\xi_0 \leqslant 5$ when $d_S/\xi_0 = 1$. For the above plots, we have used $\Delta_{\mathrm{ex}}/E_F = 0.2$.

normal layer remains intact as long as the probability of the AR is nonzero. This captures the essential physics of a two-mirror Fabry-Pérot resonator with a resonator length $2d_N$, which we shall describe now. The N-FI and S-N interfaces operate as "mirrors" for the QPs that give rise, respectively, to a spin-dependent specular reflection (a spin-dependent mirror) and a phase-conjugating mirror, which retroreflects electrons with energy $E_F + \varepsilon_A$ as holes with energy $E_F - \varepsilon_A$ [24]. The resonant enhancement of a Fabry-Pérot device occurs when its mirrors have a near unity reflection probability [25]. Here, the N-FI interface reflects all the incident QPs with probability 1, while the retroreflection probability of the S-N interface, on the other hand, is determined by the AR probability. Therefore, the Fabry-Pérot enhancement is in accordance with the AR amplitude, which for an S with a thickness d_S [15] is given by

$$r_A = \frac{(1-\gamma) r_A^{\infty}}{1 - \gamma (r_A^{\infty})^2}. \tag{5}$$

For subgap energies, in the limiting case of $d_S > \xi_0$, we get $\gamma \ll 1$ or equivalently $|r_A| \approx 1$, for which the resonant enhancement of a Fabry-Pérot device is expected. For energies above the gap, on the other hand, the AR reflection amplitude decreases. This results in highly transmitting channels near $\varepsilon \gtrsim \Delta_0$, which rapidly decline for higher energies (see Fig. 3).

In addition to the QP interference in the normal layer (Rowell-McMillan resonance), which leads to the mixing conductance oscillation, above the gap a quantum interference inside the S layer can take place. An incident electronlike QP interferes with a holelike QP reflected from the other S-N interface, which may result in $|r_A| = 0$. The process known as Tomasch oscillations [26] occurs for QP energies $\varepsilon_n/\Delta_0 = \sqrt{1 + (n\pi\xi_0/2d_S)^2}$ with integer n, which modulates the amplitude for the Fabry-Pérot oscillations. The Rowell-McMillan and Tomasch based geometric resonances of $\mathrm{Re}\, g^{\uparrow\downarrow}$ are shown in Fig. 3.

III. SPIN-PUMPING ENHANCEMENT

The spin pumping is generated by the variations in the magnetization direction $\boldsymbol{m}(t)$ [3,10,27]. For sufficiently slow variations, to the first order in the pumping parameter frequency $|\partial_t \boldsymbol{m}|$, the spin pumping can be written in terms of the instantaneous mixing conductance in the magnetization coordinate system, that is, Eq. (2). Consequently, the spin-pumping current, assuming no voltage bias [18], is given by

$$\boldsymbol{I}_s(t) = \frac{1}{4\pi} g^{\uparrow\downarrow}_{\mathrm{eff}}\, \boldsymbol{m} \times \partial_t \boldsymbol{m}, \tag{6}$$

where the effective mixing conductance is defined as follows:

$$g^{\uparrow\downarrow}_{\mathrm{eff}} \equiv \int_{-\infty}^{\infty} d\varepsilon\, \partial_{\varepsilon} f(\varepsilon)\, \mathrm{Re}\, g^{\uparrow\downarrow}. \tag{7}$$

Here, $f(\varepsilon) = (1 + e^{\varepsilon/k_B T})^{-1}$ is the Fermi-Dirac distribution and in order to properly take into account the temperature dependence of the S order we have considered a temperature-dependent S gap $\Delta(T)$ [21].

In accordance with Eq. (6), the spin-pumping current in the direction of $\boldsymbol{m} \times \partial_t \boldsymbol{m}$ is simply determined by $g^{\uparrow\downarrow}_{\mathrm{eff}}$, which can be regarded as the mixing conductance in the temperature domain. In order to focus on the role of ABS resonances, we have defined normalized effective conductance $\tilde{g}^{\uparrow\downarrow}_{\mathrm{eff}} \equiv g^{\uparrow\downarrow}_{\mathrm{eff}}(d_S)/g^{\uparrow\downarrow}_{\mathrm{eff}}(d_S = 0)$. Here, $g^{\uparrow\downarrow}_{\mathrm{eff}}(0)$ yields the effective conductance in the normal state. The resultant normalized conductance is plotted in Fig. 4. We find that, for subgap temperatures, $\tilde{g}^{\uparrow\downarrow}_{\mathrm{eff}}$ shows a significant enhancement at the finite thickness of the S layer, i.e., $d_S \sim \xi_0$. The enhancement is optimal at the midgap temperatures and diminishes down to unity (the normal case) upon approaching T_c.

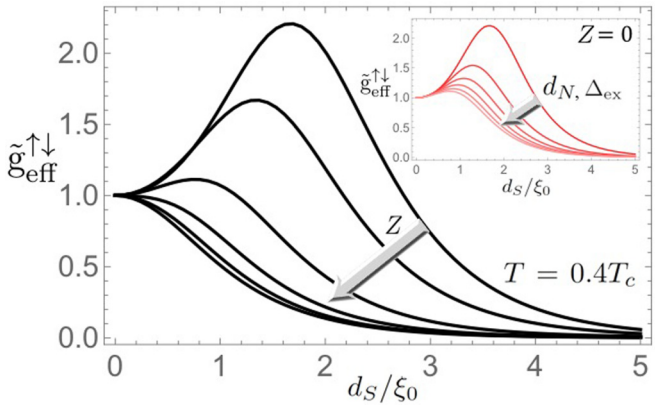

FIG. 5. The normalized effective conductance is shown for various barrier potential strengths Z, which are plotted by increasing Z in increments of 0.5 from 0 to 2.5. The enhancement feature ceases to exist for strong barriers $Z > 1$. The inset plot shows that the simultaneous increase of d_N and $\Delta_{\rm ex}$ with $Z = 0$ can account for the conductance in the weak barrier case $Z < 1$. The red plots are generated by simultaneously increasing both the exchange interaction $\Delta_{\rm ex}/E_F$ from 0.1 to 0.6 in increments of 0.1 and d_N/ξ_0 from 3 to 4.5 in increments of 0.3. In the above plots, we have set $d_N/\xi_0 = 3$, $\Delta_{\rm ex}/E_F = 0.1$.

Before closing this paper, we explore the effect of a barrier potential at the S-N interface. Physically, this can originate from a thin oxide layer or a localized disorder on the interface. The essential effects of the interfacial scattering, caused by this layer, can be captured by a potential of the form $Z\hbar v_F \delta(x - d_S)$, where the dimensionless parameter Z determines strength of the barrier. Here, v_F is the Fermi velocity and $\delta(x)$ is the Dirac delta function.

At the S-N interface, a nonzero Z results in reduced transmission and AR probabilities by introducing ordinary electron and hole reflections [28]. This partially reflective interface can lead to the formation of normal bound states localized in the N layer. In contrast, the case of zero barrier ($Z = 0$) leads to ABSs only. For subgap energies, with the increase of Z the ordinary reflection probability surpasses the AR probability [28], which leads to ABSs to be pushed away from zero (towards the continuum of states above the gap) and replaced with ordinary bound states [15]. Consequently, in the strong barrier limit $Z > 1$, the subgap transport channels are due to the normal bound-state resonances, where superconductivity suppresses the spin pumping (see Fig. 5). We point out that the effective conductance is normalized with respect to $g_{\rm eff}^{\uparrow\downarrow}(d_S = 0)$, which accounts for the contribution of the normal bound-state resonances. The weak barrier limit ($Z < 1$), on the other hand, can effectively be described within the zero-barrier limit by an increased d_N and $\Delta_{\rm ex}$ (due to the multiple ordinary reflections) [see Fig. 5 (inset)].

IV. CONCLUSION AND DISCUSSION

We have shown that superconductivity can greatly affect spin pumping due to the formation of the resonant ABSs, which result in highly transmitting spin transport channels when $d_S \sim \xi_0$. This can be manifested experimentally by an increase in Gilbert damping of the FI dynamics. The Gilbert damping enhancement in an NbN-GdN structure has been observed to peak for subgab temperatures [5], where NbN is an s-wave superconductor with coherence length of $\approx$5 nm that is adjacent to a ferromagnetic-insulator film, GdN. The enhancement takes place for $d_S = 10$ nm and it is suppressed for $d_S = 2$ nm. We believe that this is in good agreement with our results (e.g., Fig. 4). On the other hand, unfolding N_r-S-N-FI effectively maps our setup to an N_r-S-F-S-N_r structure, where F stands for a normal metal with a ferromagnetic order. The hybrid structure N_r-Nb-$Ni_{80}Fe_{20}$-Nb-N_r studied in Ref. [4] shows a significant spin-pumping enhancement only when the Nb thickness is roughly equal to its coherence length ($d_S \approx \xi_0 = 30$ nm). In order to reveal a large enhancement, they have utilized a range of spin-sink materials N_r with spin-orbit interaction, such as Pt, W, or Ta. In Ref. [17] the same hybrid structure of Ref. [4] has been used except for a particularly magnetized spin sink Pt/Co/Pt. It is shown that the spin-pumping efficiency across Nb is tunable by controlling the magnetization direction of Co.

Furthermore, hybrid Josephson junctions realizing ABSs with near unity transmission probability for charge transport have been proposed to coherently manipulate quantum-information devices such as Andreev-level qubits [29,30]. From this standpoint, unfolding our setup realizes a magnetically active Josephson junction [8] with resonant transport channels, which in turn can provide a spintronic paradigm for a coherent manipulation of quantum-information devices involving ABSs.

Note added. Recently, we became aware of an interesting and closely related work by Silaev [31].

ACKNOWLEDGMENTS

It is a pleasure to acknowledge discussions with C. Ciccarelli and W. A. Robinson, who drew our attention to this problem. M.T.A. wishes to thank S. Tanhayi Ahari for useful comments on the paper. This work is supported by the U.S. Department of Energy, Office of Basic Energy Sciences under Grant No. DE-SC0012190.

[1] J.-D. Pillet, C. H. L. Quay, P. Morfin, C. Bena, A. Levy Yeyati, and P. Joyez, Nat. Phys. **6**, 965 (2010); J. Schindele, A. Baumgartner, R. Maurand, M. Weiss, and C. Schönenberger, Phys. Rev. B **89**, 045422 (2014); J. A. Sauls, Phil. Trans. R. Soc. A **376**, 20180140 (2018).

[2] E. J. H. Lee, X. Jiang, M. Houzet, R. Aguado, C. M. Lieber, and S. De Franceschi, Nat. Nanotech. **9**, 79 (2014); F. Pawlicki and I. Weymann, Phys. Rev. B **98**, 085411 (2018).

[3] Y. Tserkovnyak, A. Brataas, G. E. W. Bauer, and B. I. Halperin, Rev. Mod. Phys. **77**, 1375 (2005).

[4] K.-R Jeon, C. Ciccarelli, A. J. Ferguson, H. Kurebayashi, L. F. Cohen, X. Montiel, M. Eschrig, J. W. A. Robinson, and M. G. Blamire, Nat. Mater. **17**, 499 (2018).

[5] Y. Yao, Q. Song, Y. Takamura, J. P. Cascales, W. Yuan, Y. Ma, Y. Yun, X. C. Xie, J. S. Moodera, and W. Han, Phys. Rev. B **97**, 224414 (2018).

[6] S. Kashiwaya, Y. Tanaka, N. Yoshida, and M. R. Beasley, Phys. Rev. B **60**, 3572 (1999).

[7] J. Linder and J. W. A. Robinson, Nat. Phys. **11**, 307 (2015).

[8] M. Fogelström, Phys. Rev. B **62**, 11812 (2000).

[9] M. Eschrig, J. Kopu, J. C. Cuevas, and G. Schön, Phys. Rev. Lett. **90**, 137003 (2003); G. Metalidis, M. Eschrig, R. Grein, and G. Schön, Phys. Rev. B **82**, 180503(R) (2010); H. Yang, S.-H. Yang, S. Takahashi, S. Maekawa, and S. S. P. Parkin, Nat. Mater. **9**, 586 (2010)

[10] A. Brataas and Y. Tserkovnyak, Phys. Rev. Lett. **93**, 087201 (2004).

[11] F. S. Bergeret, A. F. Volkov, and K. B. Efetov, Phys. Rev. Lett. **86**, 4096 (2001); M. Houzet and A. I. Buzdin, Phys. Rev. B **76**, 060504(R) (2007).

[12] M. Eschrig, Phil. Trans. R. Soc. A **376**, 20150149 (2018).

[13] T. Vezin, C. Shen, J. E. Han, and I. Žutić, Phys. Rev. B **101**, 014515 (2020).

[14] T. Yokoyama and Y. Tserkovnyak, Phys. Rev. B **80**, 104416 (2009).

[15] See Supplemental Material at http://link.aps.org/supplemental/10.1103/PhysRevB.103.L100406 for a discussion of multichannel scattering, exact expressions of the reflection amplitudes, and a heuristic argument for the dynamic generation of triplet pairing. We also provide a brief discussion of the ABS modification in the presence of the interface barrier potential.

[16] M. Inoue, M. Ichioka, and H. Adachi, Phys. Rev. B **96**, 024414 (2017).

[17] K.-R. Jeon, X. Montiel, S. Komori, C. Ciccarelli, J. Haigh, H. Kurebayashi, L. F. Cohen, A. K. Chan, K. D. Stenning, C.-M. Lee, M. G. Blamire, and J. W. A. Robinson, Phys. Rev. X **10**, 031020 (2020).

[18] H. J. Skadsem, A. Brataas, J. Martinek, and Y. Tserkovnyak, Phys. Rev. B **84**, 104420 (2011).

[19] B. Belchev, S. G. Neale, and M. A. Walton, Can. J. Phys. **89**, 1127 (2011).

[20] Y. Nazarov and Y. Blanter, *Quantum Transport: Introduction to Nanoscience* (Cambridge University, Cambridge, England, 2009).

[21] We consider an energy gap of $1.1E_F$ for up-spin and $1.1E_F + 2\Delta_{ex}$ for down-spin electrons. The Fermi energy E_F is assumed to be identical for the different layers, $E_F = 5.32$ eV. Furthermore, we have assumed Nb as the S with $T_c = 9$ K, $\xi_0 = 30$ nm, and $\Delta_0 = 3$ meV. We have adopted the following empirical parametrization for a temperature-dependent superconductor gap for Nb, $\Delta(T) = \Delta_0(1 - T/Tc)^{1.94}(1 + 2.17T/Tc)$, that is taken from R. C. Dougherty and J. D. Kimel, *Superconductivity Revisited* (CRC, Boca Raton, FL, 2012)

[22] A. Brataas, Yu. V. Nazarov, and G. E. W. Bauer, Phys. Rev. Lett. **84**, 2481 (2000).

[23] F. Hübler, M. J. Wolf, T. Scherer, D. Wang, D. Beckmann, and H. v. Löhneysen, Phys. Rev. Lett. **109**, 087004 (2012).

[24] H. van Houten and C. W. J. Beenakker, Physica B: Condensed Matter **175**, 187 (1991).

[25] N. Ismail, C. C. Kores, D. Geskus, and M. Pollnau, Optics Express **24**, 16366 (2016).

[26] W. J. Tomasch, Phys. Rev. Lett. **16**, 16 (1966).

[27] K. Xia, P. J. Kelly, G. E. W. Bauer, and I. Turek, Phys. Rev. Lett. **89**, 166603 (2002).

[28] G. E. Blonder, M. Tinkham, and T. M. Klapwijk, Phys. Rev. B **25**, 4515 (1982).

[29] F. Nichele, E. Portoles, A. Fornieri, A. M. Whiticar, A. C. C. Drachmann, S. Gronin, T. Wang, G. C. Gardner, C. Thomas, A. T. Hatke, M. J. Manfra, and C. M. Marcus, Phys. Rev. Lett. **124**, 226801 (2020).

[30] J. Michelsen, V. S. Shumeiko, and G. Wendin, Phys. Rev. B **77**, 184506 (2008); C. Janvier, L. Tosi, L. Bretheau, C. Ö. Girit, M. Stern, P. Bertet, P. Joyez, D. Vion, D. Esteve, M. F. Goffman, H. Pothier, and C. Urbina, Science **349**, 1199 (2015).

[31] M. A. Silaev, Phys. Rev. B **102**, 180502(R) (2020).